ENHANCEMENT OF A MODULAR AND VERSATILE UAV PROPELLER FORCE MEASUREMENT SYSTEM

C. Rieger*, A. L. Holzäpfel*, M. Hornung*
* Institute of Aircraft Design, Department of Aerospace and Geodesy (TUM), Boltzmannstrasse 15, 85748 Garching, Germany

Abstract

Designing vertical take-off and landing (VTOL) unmanned aerial vehicles (UAV) requires precise propeller data for optimization. A propeller test bench is available at the institute of aircraft design at TUM. To determine its accuracy, previous measurements were compared to public data using the same propellers. This evaluation revealed deviations and led to a complete redesign of the hardware, software as well as additions of several environmental sensors for a precise measurement. The paper describes the problems encountered at the old test bench, develops solutions to counter them and shows the current state of the refurbishment. Several propellers have been tested and their preliminary propeller coefficients are presented.

Keywords

Propeller measurement; Propeller test bench; VTOL; UAV

1. INTRODUCTION

1.1. The need for a propeller force measurement system

Adding VTOL capabilities to UAVs simplifies the usage for the end-user and opens up new possible use cases of UAVs. New market segments are gained and the demand for high efficiency UAV rises. The propellers are crucial to increase the overall UAV performance. VTOL hover propellers are especially important due to their high-power demand during hover flight. Every aircraft optimization needs propeller and motor data sets to calculate the energy requirements for the entire aircraft. High quality propeller coefficients, created in a wind tunnel, are a necessity for flight testing and validation as well. Using the air speed and motor RPM values, the real propeller thrust during the flight can be calculated. In a stationary flight this automatically equals to the drag of the aircraft. Together with the known weight of the aircraft, the lift and drag create one point in the aircraft polar.
To verify calculated propeller data and obtain the characteristics of unknown propeller geometries, a reliable and versatile propeller measurement system is required.

1.2. Static measurements

All of the following data refer to static propeller measurements, meaning no airspeed is present besides the propeller intake and slipstream. Since wind tunnel time is sparse, it requires a properly working and calibrated test bench. Static measurements represent the hover phase of a VTOL UAV and, therefore, in most cases the flight state with the highest power consumption. Optimization in this flight regime can greatly influence the overall UAV performance.

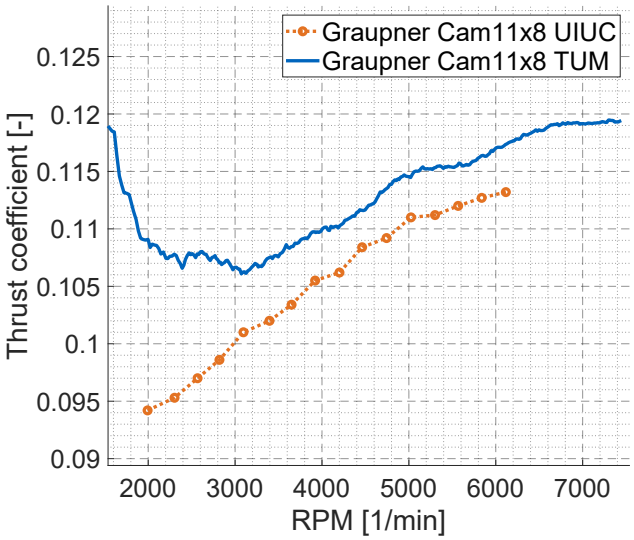

FIG 1. Thrust over RPM for a Graupner 11" x 8". The deviations between the TUM (blue) and the UIUC (orange) measurements are visible. Modified from [1]

doi: 10.25967/550030

2. METHODS

2.1. Propeller coefficients

The following definition for the propeller coefficients is used:
Thrust coefficient:

$$C_T = \frac{T}{\rho n^2 D^4} \tag{1}$$

Power coefficient:

$$C_P = \frac{P_s haft}{\rho n^3 D^5} \tag{2}$$

where n is the rotational speed in revolutions per second, D is the propeller diameter and ρ is the air density. In the following the rotational speed will be given as revolutions per minute (RPM).
All parameters on the right side of equations 1 to 2 need to be measured or derived from measurement values. [2]

Thrust / Torque

The main parameters are thrust and torque. Both are mechanical forces, produced by the rotation of the propeller. The motor creates an equal but opposite moment and transfers the trust to its mounting point. A measurement device attached to the mounting point can record the acting forces and moments.

Air density

The Air density can be calculated using Temperature, relative humidity and pressure from installed sensors:

$$\rho = \frac{p}{R_f * T} \tag{3}$$

with

$$R_f = \frac{R_S}{1 - \varphi * \frac{p_d}{p} * (1 - \frac{R_S}{R_d})} \tag{4}$$

and

$$p_d = 6.112 * exp(\frac{17.62 * T}{243.12 + T}) \tag{5}$$

Rotational speed

The rotational speed can be measured by different methods: A photo sensor recognizing the turning of the propeller blade or a marking on the motor, a magnetic sensor with a magnet on a rotating part or an electric RPM sensor counting the electric field rotations of one of the three motor phases of a brushless DC motor.
For measurements with an electric RPM sensor, the rotational speed can be calculated by

$$RPM = \frac{f * 60}{p} \tag{6}$$

where p is the number of motor pole pairs of the brushless motor. The precise measurement of the rotational speed is important as it will affect the thrust and power coefficients exponentially to the second and third power, respectively. (Formulas 1 and 2)

Propeller diameter

The propeller diameter is fixed and defined by the manufacturer of the propeller. Alternatively, it can be easily measured once before the measurement campaign.

2.2. Public data sources

The most comprehensive research on the performance and efficiency of propellers at low Reynolds numbers has been conducted at the University of Illinois at Urbana-Champaign by the research group of Michael Selig. In 2011 Brandt and Selig tested 79 two-bladed propellers in the diameter range of 9 inches to 11 inches. In 2014 Deters et al. tested propellers in the 2.25 inches to 9 inches diameter range in the same set up [3]. In 2020 Dantsker et al. measured thrust and power coefficients for 40 two-bladed Aeronaut-CAM carbon folding propellers with a diameter range of 9 inches to 16 inches [4]. The results of these measurements are available on the UIUC Propeller Data Site [5].
A similar test bench was built at the University of Beira Interior in Portugal by Silvestre et al. to measure propellers up to 14 inches for their own research projects. They extensively compared their results to those of UIUC [6]. They found mostly consistent results; however, they observed small variations such as a negative offset in the power coefficient at certain rotational speeds with one propeller or a positive offset in the thrust coefficient with another. The two previous experimental set-ups included a T-shaped pendulum concept for the thrust measurement. A different set-up exists at the Wichita State University. The load cell is directly mounted to the propeller and a steel C-strut. Their propeller test bench was first built and used by Merchant and Miller in 2006 and can measure propellers from 6 inches to 22 inches in diameter [7]. Ghoddoussi used the same test rig in 2015 to test further propellers to validate his propeller analysis [8]. He also compared his results to those of the UIUC and found that they agree with each other. McCrink and Gregory developed a performance model using the Blade Element Method [9] and also acquired data for three different propellers to verify their analytical results. All of the above-mentioned universities conducted their experiments in a wind tunnel and hence, received dynamic thrust and power coefficients for different advance ratios. Solely, the UIUC acquired data for static conditions. They were however acquired with the test bench being placed in a wind tunnel and no information on the remaining airflow produced by the propeller is available. [2]

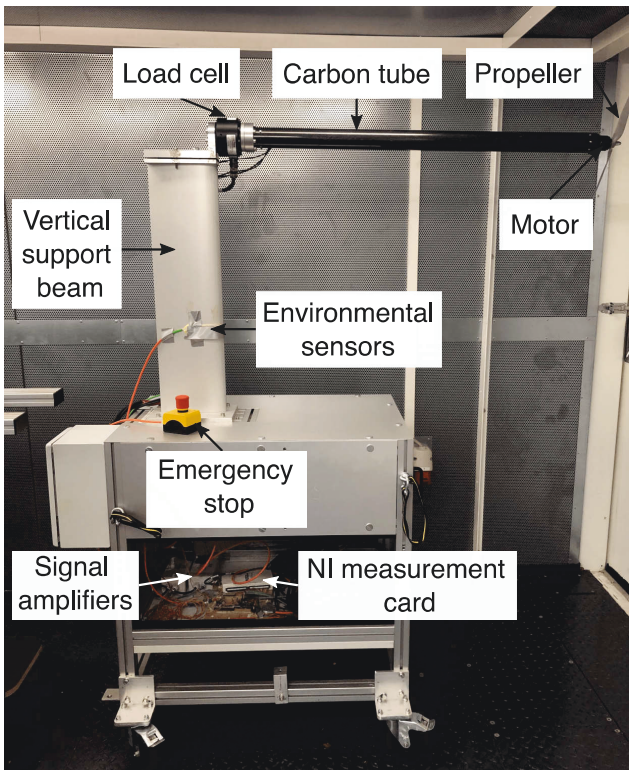

FIG 2. Test bench inside the measurement container with labels of the most important components, already including some additions. [2]

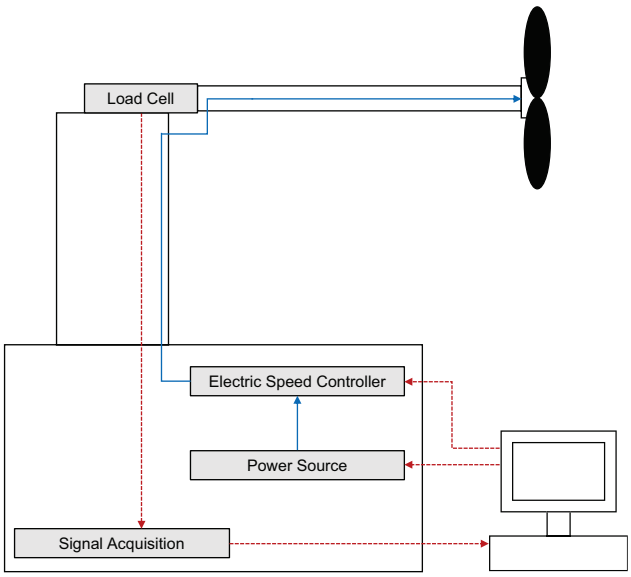

FIG 3. Simplified sketch of the test bench. The dashed lines represent the flow of information and the solid lines the power cables. [2]

2.3. Available Hardware

The original test stand used at the Institute of Aircraft Design at TUM was built in 2015 [10]. The goal of the test bench is to measure torque, thrust and rotational speed of the propeller. Automated measurement of environmental data like air density was not included.

2.3.1. Design and Components

The test rig consists of a mobile stand which contains a 15 kW direct current (DC) power supply, signal amplifiers and the data acquisition and control systems. A vertical support beam is mounted on top. A mounting bracket holds the load cell. A soft tissue is placed between the two components to dampen oscillations. The load cell is connected to a mount where the motor is fixed. The test bench can be seen in Figure 2 with the respective labels and in Figure 3 as a rough sketch. In the picture visible is also a long black CFRP tube extending over 1 m towards the motor. This is an optional structure that can hold bodies into the slipstream of the propeller to measure its effects on the propeller.
A variety of sensors are implemented in the test bench. The Axial Torsion Load Cell Model 1216 from Interface Force [11] measures the thrust and torque forces using strain gauges. It has a capacity of 2.22 kN and 28.2 N m. The load cell requires two signal amplifiers, one for the axial and one for the torsion loads. A voltage divider and a Honeywell current sensor are implemented at the power supply output. A SM Modellbau brushless revolution sensor [12] acquires the RPM values. [2]
A National Instrument (NI) USB-6211 multifunction I/O device is used as data acquisition device. It acquires the analog voltage data from all sensors.

2.3.2. System Description

The power supply provides DC power to the ESC which drives the motor. The commanded rotational speed for the ESC is controlled by the a Pololu Maestro 6-channel servo controller [13] which receives its commands from the measurement computer. The rotation of the propeller results in torque and thrust which are measured by the load cell. The signal from the load cell is amplified, acquired by the NI measurement card and sent to the computer. The measurement card also acquires the signals from the current and voltage sensors which are placed directly after the power supply. A sketch of the interconnection between the key components is pictured in Figure 3.

2.3.3. Software

The control software is written in MATLAB with a graphical user interface (GUI) for the user interaction. All data are measured by the NI USB acquisition card and transferred to the measurement computer. The MATLAB software converts the acquired analog voltage data to physical forces, moments and temperatures. The RPM signal is analyzed with the help of a Fast Fourier Transformation (FFT) to obtain the main frequency. This is then transferred to a rotational speed. All processed data are then saved to a file.

2.4. Sampling Theorem

Sampling is the acquisition of an analog signal at discrete time intervals. Mathematically, it can be seen as a multiplication of the analog signal $x(t)$ by a periodic impulse train $p(t)$ that has the sampling period T_s [14].

$$x_p(t) = x(t)p(t) \tag{7}$$

where

$$p(t) = \sum_{n=-\infty}^{\infty} \delta(t - nT_s) \tag{8}$$

The maximum frequency in the analog signal f_{max} determines the sampling frequency F_T with which the signal needs to be sampled such that an accurate reconstruction is possible. The sampling theorem states that the sampling rate F_T is required to be at least twice the highest possible frequency in the analog signal [14].

$$F_T \geq 2f_{max} \tag{9}$$

$2f_{max}$ is called the Nyquist rate. If the sampling theorem is violated, higher-frequency content in the analog signal might take on the false identity of a lower frequency in the resulting discrete series [15]. [2].

2.4.1. Linear Regression Analysis

A regression analysis is used to establish a relationship between a set of independent and dependent variables [15]. The independent variable can be altered separately from all other variables, whereas the dependent variable is affected by changes in independent variables. It is assumed that no deviations are present in the independent variable but only in the dependent one. [16]. A regression analysis is often used in calibrations where the input value is precisely known. Furthermore, it is assumed that the variation in the measured, dependent variable follows a normal distribution at each fixed value of the independent variable [15]. [2] A more detailed explanation of the used regression analysis can be found in [2].

2.5. External hardware

To check for errors during the measurement, several external measurement devices are available. The Unilog2 by SM-Modellbau allows the recording of current, voltage, RPM and temperature. It is commonly used as measurement unit in model aircraft, but has no certification or calibration.
A handheld sensor Uni-T UT 372 allows for RPM measurements with an accuracy of ±(0.04 % + 0.2) 1/min in the relevant range between 1000 RPM and 10000 RPM.
A standard oscilloscope eases the work during noise debugging and calibration of supply voltage and output voltage of the load cell amplifiers.

3. CONDUCTED WORK

3.1. Requirement analysis

The requirements are based on the problems encountered during the previous use of the test bench. A short description of the encountered problems and the desirable goal is given respectively.

3.1.1. Requirements - Entire system

- Versatile use
  The original test bench already offered different mounting possibilities for various motors. This enables a fast adaption for new power trains. Small motors however could only be mounted to the long CFRP boom from the slipstream measurements. While maintaining the available versatile measurement capabilities for large motors, an additional support for small motors was required.
- Easy to upgrade
  Since the test bench is still in development and testing, a lot of upgrades and redesigns are expected. Making the system capable of integrating new measuring modules fast and with a minimum amount of changes to the entire test bench, makes this faster and more reliable.
- Easy to modify
  Measurements and modifications are often realized in cooperation with students or coworkers with little experience with the test bench. Making every component as simple as possible and keeping it separated from other components reduces the necessary training time.

3.1.2. Requirements - Hardware

- Improvement of electrical circuits
  Due to the centralized recording of all data by the NI USB data acquisition box, several sensors had multiple connections to ground, creating ground loops that could alter the data and introduce noise into the system. These loops had to be removed.
  The cables transporting precise voltages need shielding against external influence. This was especially important for the outputs from the load cell amplifier. The large range of the load cell and only a limited output voltage range creates only small voltage differences for the used propellers. This makes the measurement prone to interference effects.
- Power supply
  Earlier tests in a wind tunnel showed that there is significant back-current from the ESC to the power source if the propeller is acting in windmill mode at higher wind speeds. The installed power supply does not act as a sink. An outlet for the excess voltage created by the back-current is needed to prevent damages to the electronic components.
- Adding environmental sensors
  Environmental measurements to calculate the air density had not been implemented yet. A manual

recording before and after measurements showed that these values change significantly during the measurement. Especially when the sun was shining on the roof of the measurement container, the air heated up during test pauses and cooled down quickly as soon as the running propellers sucked in fresh air from outside. Additional sensors for air temperature, humidity and pressure make it possible to obtain the correct air density during measurements.

3.1.3. Requirements - Software

- Stable software
  The software was initially created in MATLAB 2013, creating some compatibility issues with newer versions. A GUI was used to interact with the user during planning, testing and postprocessing. While providing a consistent look, the necessary performance could not be provided. The minimum recording frequency was around 10 kHz for the RPM (FFT) analysis to work. (Section 2.3.3)
  The high data rate created a lag in processing user inputs. This even created a safety issue: Stopping a running measurement was only possible by using the hardware emergency shutdown. The software stop function was delayed for several seconds.
- Modularization
  While a unified software environment with a GUI has its advantages for an end user, development, debugging and versatility has to be reduced to keep the user interface clear. In a research environment with always changing demands, this meant too much of a constraint. Dividing the software into parts makes it easier to modify it since only the transfer values are defined between the software parts. For each part of the measurement campaign, a program is needed: to plan the measurement, conduct it while recording the data and post-process the data afterwards.
- Eliminating live calculations
  One of the reasons for the big demand of computing power and data size was the calculation of the RPM by using an analog input and an FFT analysis afterwards. RPM values are needed to ensure that the maximum rotational speed is not exceeded during testing. A different measurement method is therefore required. Other live calculations can be reduced to an approximation to give the operator enough data during the measurement, but not post-processing the data right away.
- Reduction of recorded data
  By reducing the minimum sampling frequency, a lot of data space can be saved. This makes data handling easier and post processing faster. Another reduction of saved raw values can be achieved by separating high-speed and low-speed sensors. (The environmental data like ambient temperature cannot change as fast as the RPM or thrust data.)
  While data reduction is important, there must not be aliasing due to a violation of the Nyquist rate.

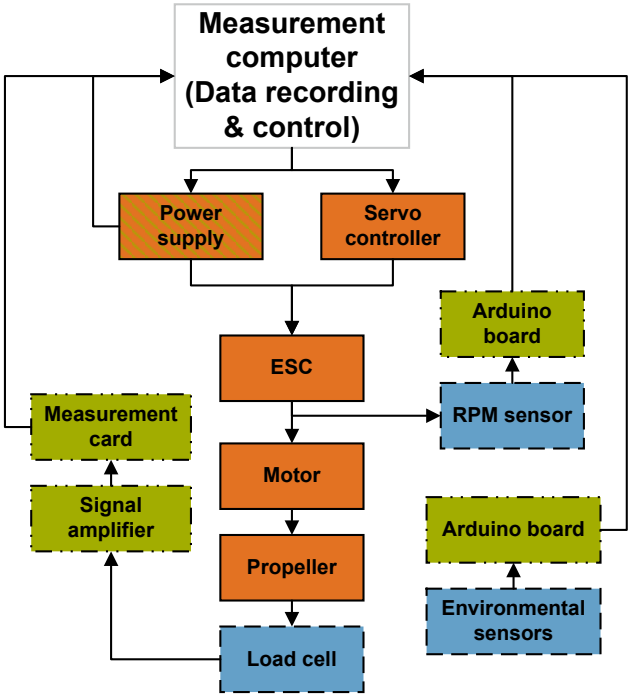

FIG 4. Schematic of the refurbished test bench. It contains the measurement computer and three types of components: the measurement object and the powering components in orange (solid line), the sensors in blue (dashed line with points) and the data acquisition components in green (dashed line)

3.2. Hardware additions and modifications

Figure 4 shows the final configuration of the modular propeller test bench. The direction of data and power flow is shown with the arrows. The middle and left part of the component structure had only minor changes to the previous test bench revision. The measurement computer is the central commanding and recording unit. The commands are given to the servo controller and power supply that drive the propeller. The forces and moments are then measured and transferred back to the computer. A new power supply sends back power data as well instead of the previous used seperate sensors. An Arduino microcontroller board was created for the RPM sensor, that was previously recorded by the NI measurement card, and the new environmental sensors that did not exist before. All hardware changes are described in more detail in this section.

3.2.1. New sensors

All new sensors were selected based on their accuracy and availability. For a quick and easy prototyping, it was decided to only use sensors with available breakout boards.
A STM LPS25H [17] pressure sensor was chosen due to its good accuracy down to ±0.2 mbar and a typical RMS noise of 0.01 mbar.
The Sensirion SHT31D [18] humidity sensor measures the relative humidity with up to ±2 % accuracy.

To get a high accuracy on temperature, a TMP117 [19] offers 16bit resolution and up to ±0.1 °°C accuracy.
A digital I²S microphone (Knowles SPH0645LM4H) was added for future use. Unfortunately, the processing of sound in a microcontroller was found to be more complex than expected.
Additional external temperature sensors can be attached to a one-wire bus. Maxim Integrated DS18B20 sensors are in use to measure 5 temperatures on the motor mount, load cell and test bench structure. They offer acceptable accuracy with a small form factor and simple wiring.

3.2.2. Additional RPM sensors

Two additional RPM sensors were installed. This means every one of the three motor phases was used for the RPM measurement instead of only one. By tripling the amount of impulses per time interval the accuracy of the measurement has been improved. The microcontroller calculates the frequency of incoming RPM impulses between data transmissions to the computer. The frequencies f obtained by the three different RPM sensors can be averaged to compute the RPM value (Formula 6).

3.2.3. Power supply

A new bi-directional power supply allows for reverse current, generated by motor braking. This is especially important for safety reasons (fast motor stop) and wind tunnel use. The Delta Elektronika SM15K is able to handle 15 kW of power continuously (max 70 V / ±450 A). A USB interface allows programming and value measurement over serial SCPI communication.

3.2.4. Cabling

Figure 5a shows the thrust voltage raw data as initial state before the removal of noise sources. The cabling between the load cell amplifiers and the NI measurement card was replaced with shielded CAT Network cables. Additionally, a separate Voltage measurement of the supply voltage is connected to the NI measurement card via a voltage divider and again, shielded CAT cables. The current sensor was found to introduce a lot of noise due to a malfunction or incorrect power supply. Since the new power supply is able to measure all relevant power data with an adequate data rate of up to 20 Hz, the necessity for a separate power sensor ceased to exist. Removing power sensor, RPM sensor and temperature sensor from the NI card reduced the measurement noise drastically.

The newly introduced sensors (Section 3.2.1) are connected to a close by microcontroller. This reduces problems with interference on the data bus. All environment sensors are on the same PCB with only the RPM sensors and the external DS18B20 temperature sensors connected externally.

3.2.5. Load cell amplifier

After the electrical wiring was cleared from ground loops and shielded wires were introduced, the load cell still created a noisy signal. The load cell signal amplifiers used output range of −5 V to 5 V for the full scale of the load cell, resulting in a low voltage output for the measured thrust and torque. Measuring these low voltages precisely was not possible with the available hardware. An option was activated to double the output range to −10 V to 10 V. The NI USB card is able to handle the higher input voltage. The accuracy of the NI card is better relative to the measured values and interference into the cabling is less critical.

The signal amplifiers contain a second order low pass filter that can be used to improve the performance and output signal quality in electrically noisy environments [20]. It is also used to ensure that aliasing does not occur in the analog-to-digital conversion. The desired sampling rate for the NI data acquisition system was 100 Hertz and thus according to the sampling theorem, the maximum frequency in the analog signal was allowed to be 50 Hertz. Therefore, the low pass filters in the signal amplifier were adjusted to a cut-off frequency of 50 Hertz. Figure 5c shows the reduction of noise by the use of the low pass filter compared to the raw data without the application of a filter in figure 5b. Measurements without a filter such as in figure 5b may even be incorrect as the sampling theorem is violated with the 100 Hz sampling rate and possible higher frequency input frequencies. [2]

3.3. Software modification

3.3.1. Modular sensor boards

RPM as well as environmental data are collected by a microcontroller board. Both of them are compatible with the Arduino programming language. This makes setting up the programming environment for future modifications and additions by other users faster. Available programming libraries to address the sensors ease the way to a working module.
The power source uses the serial connection with SCPI communication. It is text based and directly user readable. This was the inspiration to use the same kind of communication for the self programed sensor boards as well. While it needs more data rate than using a bitstream, the advantages to the user were rated more important. Deviating from SCPI standard is the return of all collected sensor values at once to save some bandwidth and processing power in the microcontroller.

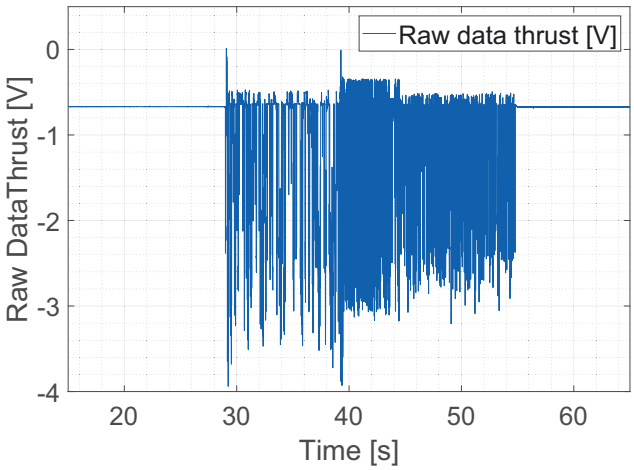

(a) Original state before modifications

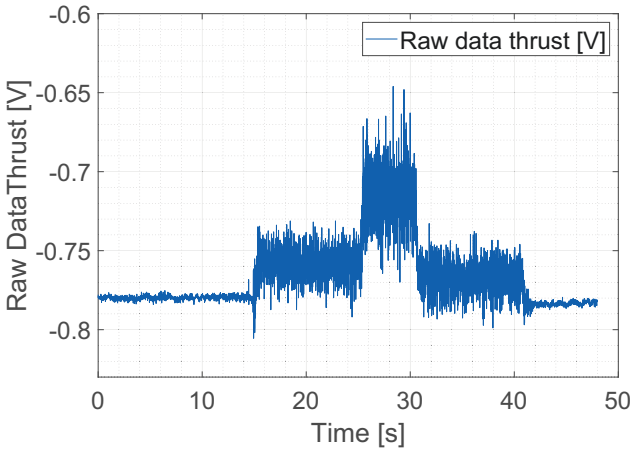

(b) Noise sources removed, no anti-aliasing filter applied

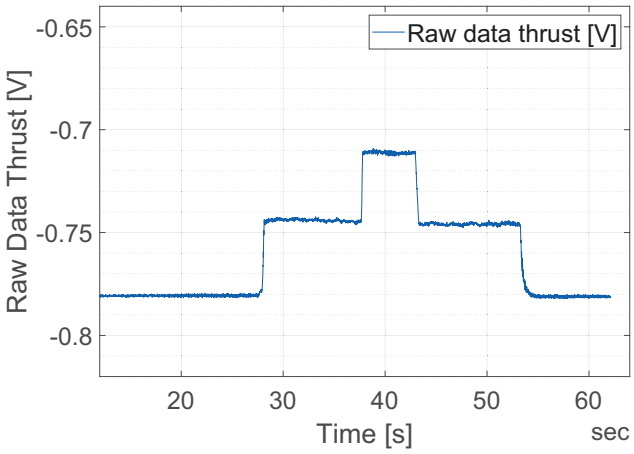

(c) With a 50 Hz cut-off frequency

FIG 5. Thrust measurement results before modification, without anti-aliasing filter and with a 50 Hz cut-off frequency low pass filter. Modified from [2]

3.3.2. Measurement planning / Test bench input file

The input file controls the complete measurement. It consists of a comma separated text file with all relevant input parameters:

- Power source
  - Voltage
  - Maximum current
  - Maximum power
  - Source mode (CC/CV/CP; Source/Sink)
  - maximum negative values when acting as a sink
- Servo/ESC command (multiple servos possible)
- Duration for the given command line

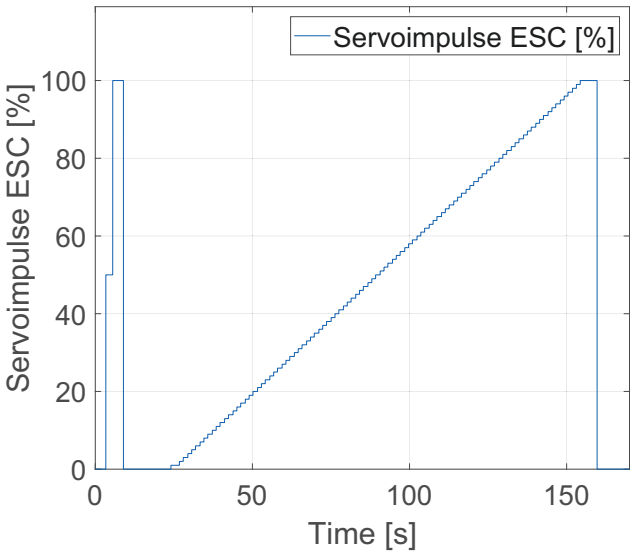

FIG 6. ESC PWM input similar to the procedure performed with the old measurement system.

This allows for a very flexible generation of new measurement procedures as well as additions like more servo outputs.
To allow comparative measurements with the old test bench, an input file was written that recreates the same commands. Static values for the power supply are used and ESC command values rise from 0 % to 100 % with defined steps. After reaching 100 %, a downward slope back to 0 % finishes the measurement. As with the old measurements from [1], this was found to create a lot of peak motor heating and was therefore changed to a shorter version with only the first half of rising ESC command values. (Figure 6)
A new 'random' input file was created with pauses between each ESC command value that shall be measured. The ESC command values were almost randomly mixed (Figure 7).
The initial short peak to 100 % in both input files was used to initialize the ESC with the used maximum PWM range to get comparable results with every measurement.

3.3.3. LabVIEW re-design

The functionality of the software is focusing on the core functionalities: Commanding the given data from the input file to the test bench, saving raw measurement data and basic monitoring functions.
The measurement software controls and records the entire process. It sends the commands of desired voltage, maximum current and power settings to the power source and the ESC command in percent to

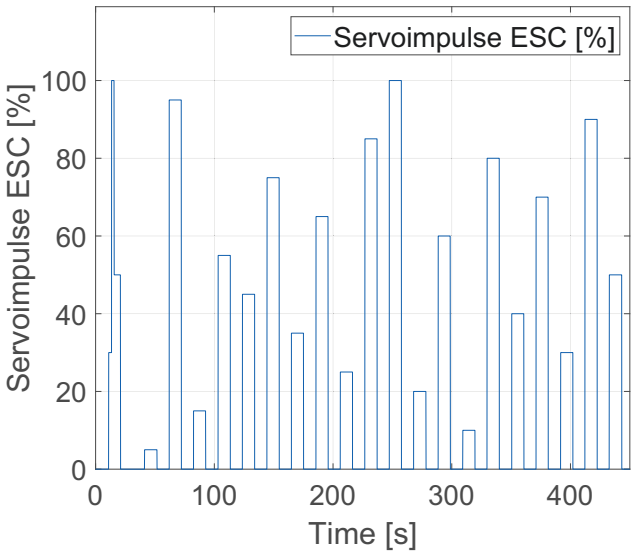

FIG 7. New random ESC input.

the servo controller board. Collecting the thrust and torque measurements from the NI measurement card is managed by an NI Express-VI block. Data requests to the other data sources of environmental data, RPM data and power source are periodically generated. The returning data is then collected and saved in individual files for every source. Every data stream has its own acquisition part in the LabVIEW program and is interconnected with the other parts as little as possible.

To avoid a simultaneous use of the power source by the command and the measurement parts, a semaphore system was introduced.

The input commands are polled line by line and processed accordingly. The design of the software allows for a flexible use of the input files up to the maximum rate at which the inputs are processed and sent by LabVIEW. Tests of the processing speed showed no relevant delay, allowing input files with a high frequency.

It was found that the Express VI blocks used initially for writing the data stream to a file, are easy to use but very inflexible. The functionality of these Express-VIs was transferred to self-programmed functions, allowing for a more adapted data structure. Live diagrams and values are shown to the user to ensure high data quality during the measurement. Converting the raw values was done by simple mathematical tasks. No processing intensive filtering or data smoothing takes place. During testing it became obvious that the monitoring of the motor efficiency helps the user. Inconsistencies with the torque or RPM values were visible in this dataset more easily. In this case a cross connection between the RPM data acquisition, Power source and the NI Acquisition (Torque) was necessary to calculate the motor efficiency. None of the live processed data, but only the raw data gathered by the sensor modules, are saved. An additional file with an overview over the measurement is currently in testing. It records all relevant general data:

- Date of the measurement
- All file names of the measurement
- Motor name
- Propeller name
- Comments describing the measurement

This eliminates the need for external lab notes.

3.3.4. Reduction of file sizes

Due to the modular design, the data polling rates of all modules are easily changeable by the user in the LabVIEW program. No changes in microcontroller software is necessary. This means that only the needed data rate for the use case can be selected, reducing the file sizes to a minimum. A minimum data rate of 100Hz is necessary for thrust and torque due to the Nyquist frequency and filter setup options.

3.4. MATLAB postprocessing

After the measurement is recorded, the data has to be processed before analysis. This is a multi-step process, programmed in MATLAB:

1) Load all relevant raw data files
2) Convert all data into timetables and synchronize all tables into one. Interpolate values to match the frequency of the thrust/torque data.
3) Optional: Reduce data rate
4) Convert raw values
   (a) Generate the RPM values
   (b) Calculate the air density
   (c) Convert the load cell data using user selectable calibrated datasets
5) Recognition of rotating and stopped motor state
6) Zero-offset identification (dependent on measurement procedure)
7) Smooth air density data
8) Calculate propeller coefficients
9) Optional: Smooth coefficients data

The process of determining the zero-offset as well as smoothing the dataset is quite calculation intensive. Therefore, all postprocessed data is saved to quickly open a measurement and view the results later.

3.5. Propeller measurements

3.5.1. Final measurement setup

A set of different motors and propellers was used for the test measurements:

- T-Motor U5 400kv
  - Aeronaut Folding 11" x 8"
  - Graupner cam 11" x 8"
  - Schulze SUPER 11" x 8"(should be same as the Graupner)
  - APC Sport 11" x 8"
- T-Motor MN807 150kv
  - T-Prop 28" x 9.2"

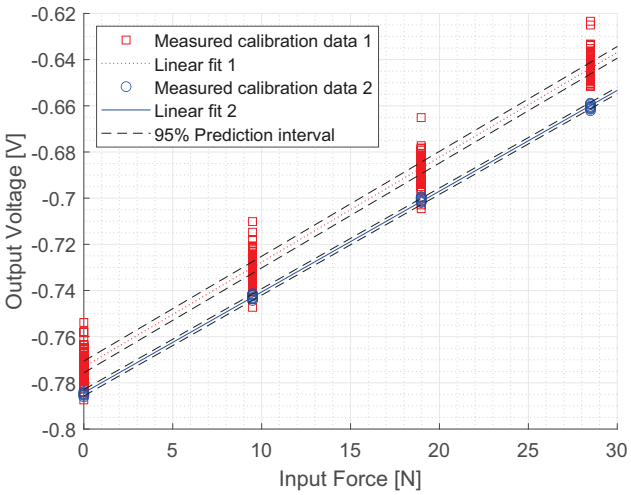

FIG 8. Two linear fits of the load cell thrust calibration with 95% prediction interval [2]

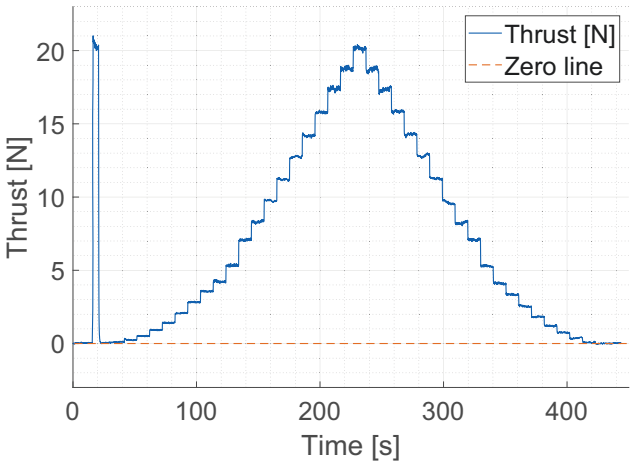

FIG 9. No observable drift of the thrust zero value, as expected. Modified graph from [2]

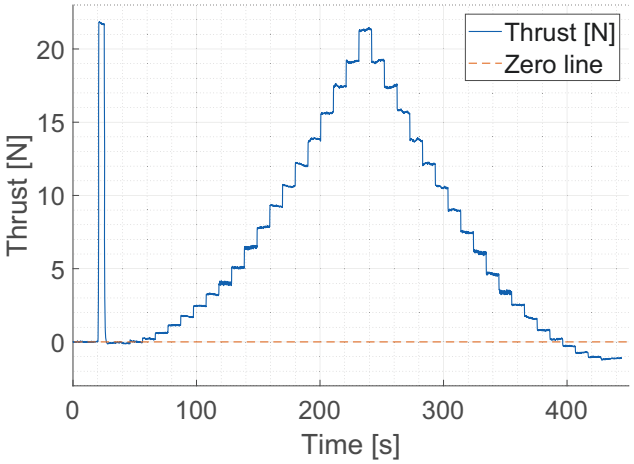

FIG 10. Drift of the thrust zero value during the next measurement. Modified graph from [2]

3.5.2. Settings

The following settings were used for the measurements:

- Data rates:
  - NI thrust/torque measurement: 100Hz
  - Environmental sensors: 2Hz
  - RPM sensor: 20Hz
  - Power source: 10Hz
- Measurement procedure:
  - intermittent testing (10s pause and 10s measurement)
  - ESC input values randomly mixed
- Post processing:
  - No data rate reduction
  - Smoothing spline as zero-offset with smoothing parameter 1E-07
  - Smoothing: Moving 0.5 s average for air density
  - Ignoring of the first two and last one second from each 10s measurement interval.
  - Usage of all three RPM sensors averaged to one rotational speed value

4. RESULTS

4.1. Calibration/Validation of load cell

A load of 9.5 N to 28.5 N was applied to the load cell. This is significantly less than the input range of the load cell, but the thrust values of the small propellers were expected to be approximately in this range. The corresponding output voltages were measured with the LabVIEW program at a sample rate of 100 Hertz. Two calibration runs were performed on two different days. Using the known input variables and the measured dependent output variables, a linear curve fit was determined for both sets of calibration data with a regression analysis in MATLAB. The two linear curve fits with their 95 % prediction intervals can be seen in figure 8. It can be observed that the calibration data of set one has larger variations than the one of set two. This may be related to the fact that more data points were acquired for the first set. This is reflected in the prediction intervals as well. To ensure that a linear fit was sufficient, the correlation coefficient between the input and output data was computed. It was found to be 0.9997 for the first run and 0.9999 for the second one. This indicates a sufficient fit as both values lie between 0.9 and 1, which is considered the range for a reliable relation between the output and input variables [15]. In addition, a linear relationship had also been assumed by the manufacturer. A deviation in the zero-offset was found for the two plotted linear fits, while the slope was comparable. [2]

4.2. Temperature drift

Besides possible errors during calibration, another source of deviations at the load cell were temperature drifts. While figure 9 shows a measurement without any difference in the measured zero thrust value before and after the measurement, figure 10 shows that this is not the case for every measurement. It was found that this zero-point drift is caused by temperature effects on both thrust and torque.

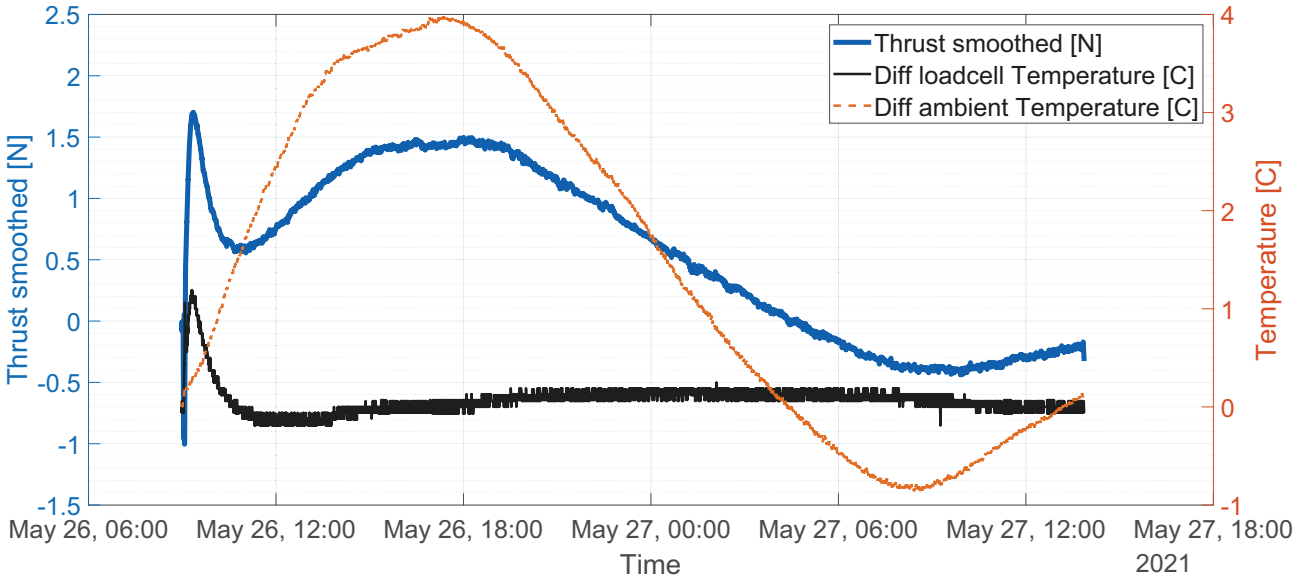

FIG 11. Differential temperature changes of ambient temperature and between front and back of the load cell, resulting in short and long term thrust zero-point drifts.

Figure 11 shows that the drift is caused by 2 different effects. One part of the drift is proportional to the ambient temperature, which can be seen in the long-term correlation (May 26, 12pm till end of measurement) between the thrust value (blue, medium) and the relative ambient temperature (orange, thin). In some situations, like a hot summer day, the location of the test bench inside a container is heated up quickly. When the measurement starts, cold air is sucked inside, cooling down the load cell that lies in the slipstream of the propeller. Isolating the housing of the load cell reduced the heat flow to the load cell due to ambient temperature changes. An in-depth research into this effect was not conducted.

The second part is a drift when the load cell is experiencing a heat flow through its housing. The heating produced by the motor was transferred back into the motor mount. This three pieced aluminum motor mount transferred the heat towards the load cell, resulting in temperature differences between the load cell force input and the load cell mounting.

Two of the DS18B20 temperature sensors were mounted on the front and back of the load cell respectively. The motor was dismounted and a heat gun replaced the motor heating to be sure that no electrical field or any electric charge from the power source, ESC or motor was responsible for the effect. In a test run the heat gun was adjusted to result in similar heating than the motor.

It can be seen in figure 11, that the temperature differences are under 1 °C while the resulting drift is over 1.5 N. This results in an unacceptable drift to accurately measure propellers with a maximum thrust of 20 N. Thermal isolation between the aluminum parts was introduced as a counter to this effect and showed some immediate improvement. The long optional CFRP boom for the slipstream measurements is a very good solution to increase the thermal resistance even more, but only suitable for small motors. Big motors with even higher heat production were impossible to mount because of structural limitations. Finally, one part of the aluminum motor mount was newly constructed out of plastics. This increased the heat transfer resistance high enough, that no more differential heating was observed.

4.3. Random input file

Another improvement was possible by the use of the new 'random' input file. A pause between the single measurement values allowed for a zero-offset compensation with very fine temporal spacing. Using this kind of sequencing improves the measurement in three ways:

1) The air cooling of the motor works better due to the reduction of peak motor heat and heat distribution over time. This leads to reduced differential heating of the load cell and, therefore, reduction of zero-point drift during the measurement.
2) A higher power setting could be achieved without motor or ESC overheating.
3) Get a new zero-offset for every measurement point

To generate the zero offset curve, all trust and torque data points without motor rotation and with a 0 % ESC value were selected. A smoothing spline was then fit to this data set. The resulting zero-offset splines were then subtracted from the original thrust or torque data. Figure 12 shows the thrust values before and after applying this method. The basic offset as well as variations during the measurement were eliminated.

4.4. Validation of RPM sensor

Investigations showed that the RPM signals from the three sensors diverged in some situations. (e.g. low to medium ESC opening with propeller attached) (Figure 13) Unfortunately, this happened quite often and based on the data alone, it was not directly

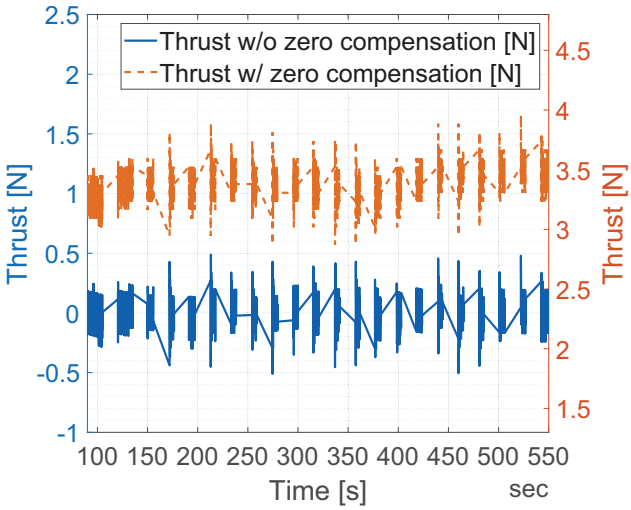

FIG 12. Effect of the zero-offset function using a smoothing spline to determine the offsets. Pictured are only the parts of the measurement when no RPM was measured and the ESC signal was at 0 %.

clear which RPM sensor is correct. The original Unilog measurement system was tested as well and resulted in similar results. Measurements with an Oscilloscope showed the expected rectangular waveform coming from the sensors. But sometimes an additional short spike was showed, effectively adding another impulse. Since this spike had a duration of less than the minimum expected length for RPM values, a digital filter was added into the RPM measuring microcontroller, only recognizing impulses with a duration of more than 100µs. This is equivalent to 300000 RPM with a 2-pole motor and more than most ESC can handle.

The Uni-T UT372 sensor was used to create independent RPM logs of a measurement. A comparison of the data in Figure 14 shows a good correlation between the 3 electrical sensors and the external optical sensor. Measurements showed a deviation between the electrical and the external optical RPM sensor of under 1 % for rotational speeds over 1800 rpm.

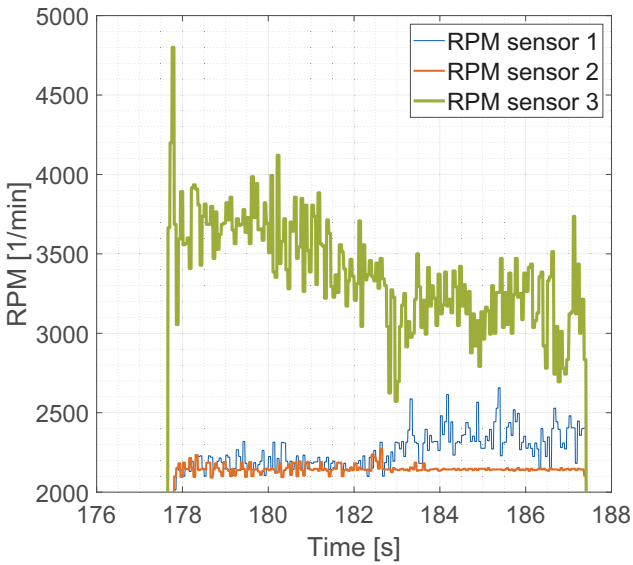

FIG 13. Example for the deviation of the RPM sensors

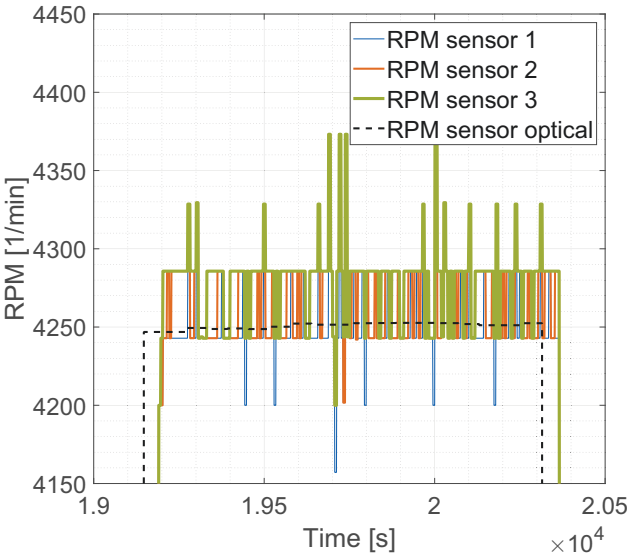

FIG 14. RPM values with improved software compared to external optical RPM sensor

4.5. Validation of environmental sensors

The environmental sensors were partly validated. The pressure sensor was compared against a public weather station on campus. The temperature sensors were compared to each other and showed little deviation. However, the reaction time of the TMP117 sensor is much faster than the integrated sensor in the SHT31D chip. The DS18B20 sensors showed a temperature offset of under 1 °C between each other.

4.6. Propeller measurement data

The following data plots show the coefficients of some of the measured propellers.

All prediction bounds show the 95 % certainty interval of the smoothing spline based on the raw data. No accuracy data from the sensor's datasheet was added. In other words, the statistical error is shown by the prediction bounds, the systematic error, precision and accuracy of the sensors is not included.

4.6.1. Aeronaut CAM Carbon Folding 11" x 8"

Figure 15 shows the typical distribution of calculated thrust coefficients. No smoothing was applied to RPM or thrust before calculating the coefficients to show the complete distribution of the obtained data by the 100 Hz thrust and interpolated 20 Hz RPM data. The smoothing spline averages the measurement points. The dotted lines display the 95 % prediction bounds for the fitted data.

A faint pattern can be seen with 'lines' from the top left to the bottom right at the lowest 3 RPM steps. These lines are predominantly caused by deviations in the RPM measurement, changing the calculated coeffi-

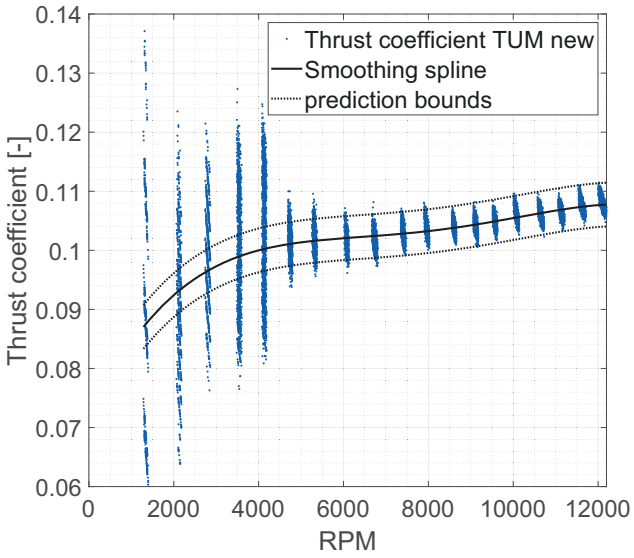

FIG 15. Thrust coefficient over RPM for the Aeronaut 11" x 8". The unsmoothed datapoints are pictured in blue. The smoothing spline in black with its 95 % prediction bounds as dotted black lines.

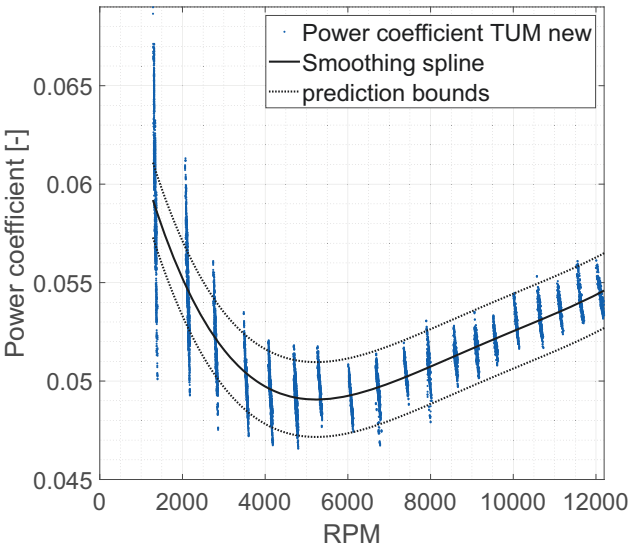

FIG 17. Power coefficient over RPM for the Aeronaut 11" x 8". The unsmoothed datapoints are pictured in blue. The smoothing spline in black with its 95 % prediction bounds as dotted black lines.

cients through Formula 1 as well, resulting in this pattern. This shows that the measurement of the rotational speed should be improved even more.
Compared to the data from UIUC there are approximately 10 % lower values for the thrust coefficient of the Aeronaut propeller. (Figure 16) The slope of the curves are however similar. A systematic error, for example a crosstalk between thrust and torque in the load cell, could be a reason for this.
The generation of the power coefficient curves is similar to the thrust coefficients. (Figure 17) The prediction bounds seem to be a little tighter compared to the thrust coefficient.

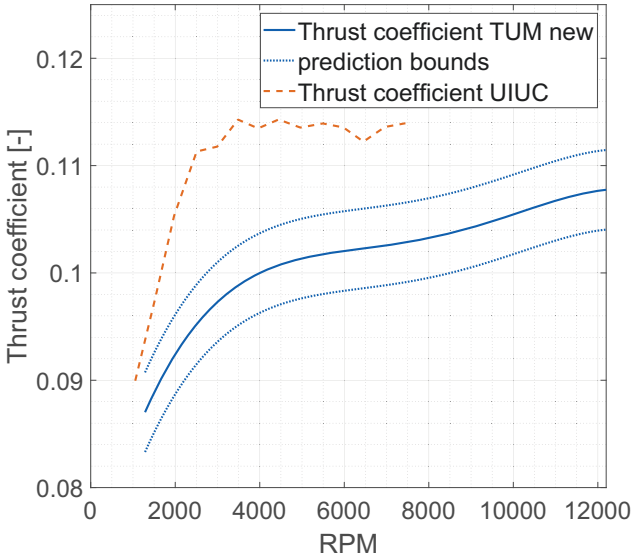

FIG 16. Thrust coefficient over RPM for the Aeronaut CAM Folding 11" x 8" (blue) with its 95 % prediction bounds as dotted blue lines. As comparison the UIUC data in orange.

Compared to the UIUC data, the power coefficient is a little bit too high and slightly shifted towards higher RPMs. (Figure 18)

4.6.2. Graupner CAM / Schulze SUPER 11" x 8"

Figure 19 shows the same propeller that was presented in Figure 1. Based on our research, the Schulze SUPER propellers are made in the same molds as the Graupner CAM Carbon (Graupner does not exist anymore). Optically they look identical besides the different manufacturer printing.
The new measurement of the Graupner propeller comes closer to the UIUC data than before in figure

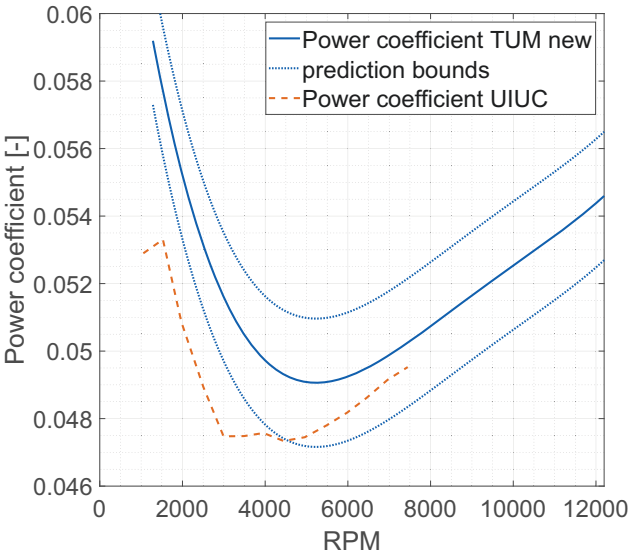

FIG 18. Power coefficient over RPM for the Aeronaut CAM Folding 11" x 8" (blue) with its 95 % prediction bounds as dotted blue lines. As comparison the UIUC data in orange.

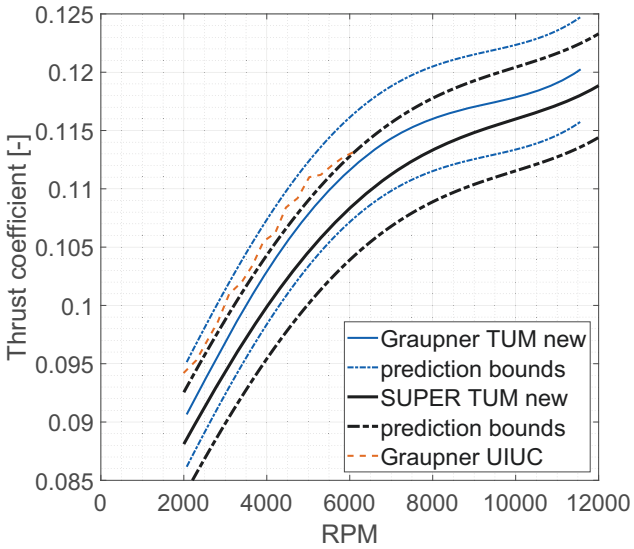

FIG 19. Thrust coefficient over RPM for the Graupner CAM 11" x 8" (blue) and Schulze SUPER 11" x 8" (black). Each with its 95 % prediction bounds as dotted lines. As comparison the Graupner UIUC data in orange.

1. The UIUC data is even within the 95 % prediction bounds. Interestingly, the measured data is now lower instead of higher. The Super propeller has a little lower thrust coefficient, but the slope of the curve is almost parallel to the Graupner measurement. It seems very likely that the propellers have the same characteristics overall.
The difference in power coefficient is even a little bit lower, showing a good correlation. (Figure 20) With this propeller, both thrust and power coefficient are lower than the data from UIUC.

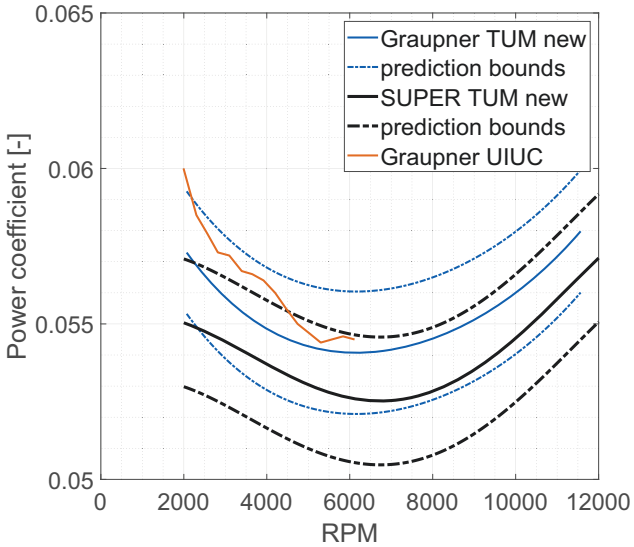

FIG 20. Power coefficient over RPM for the Graupner CAM 11" x 8" (blue) and Schulze SUPER 11" x 8" (black). Each with its 95 % prediction bounds as dotted lines. As comparison the Graupner UIUC data in orange.

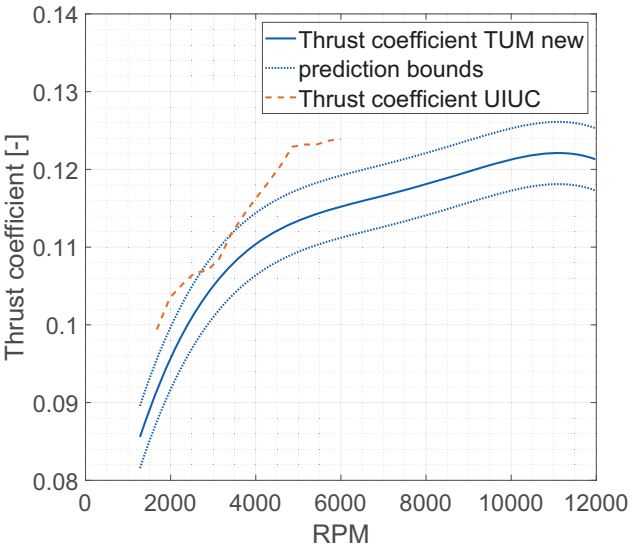

FIG 21. Thrust coefficient over RPM for the APC Sport 11" x 8" (blue) with its 95 % prediction bounds as dotted blue lines. As comparison the UIUC data in orange.

4.6.3. APC Sport 11" x 8"

The APC propeller is again a little further away from the UIUC data. (Figure 21) The kink in the UIUC thrust data at 3000 rpm is unfortunately not visible in the TUM data. The power coefficient is lower than the reference data. (Figure 22)

4.6.4. T-Prop 28" x 9.2"

Finally, a bigger propeller was mounted. With a peak power of over 4 kW, thrust of over 160 N and torque of over 5.5 N m, this propeller was using more than only a few percent of the load cell range. Unfortunately, the usual measurement environment in the container was not feasible without time intensive modifications.

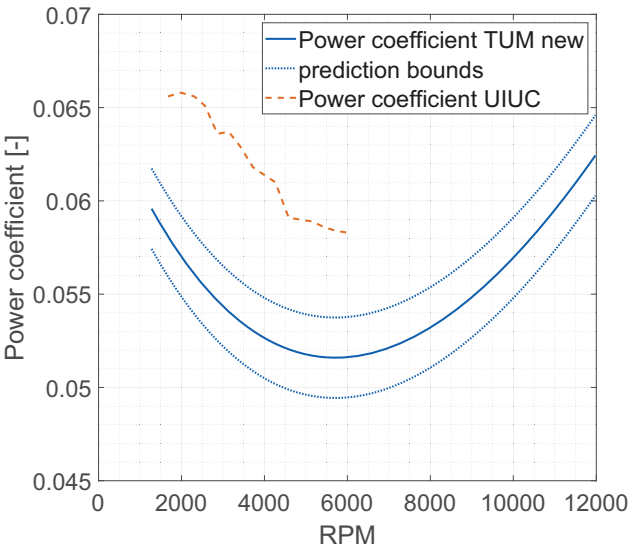

FIG 22. Power coefficient over RPM for the APC Sport 11" x 8" (blue) with its 95 % prediction bounds as dotted blue lines. As comparison the UIUC data in orange.

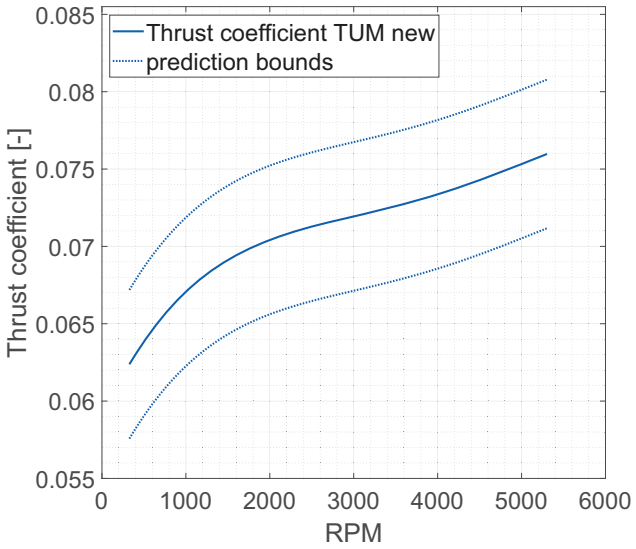

FIG 23. Thrust coefficient over RPM for the T-Prop 28" x 9.2" (blue) with its 95 % prediction bounds as dotted blue lines.

Therefore, the measurements were taken outside on a calm day. Nevertheless, some more influence by wind is expected. The thrust coefficient has quite large prediction bounds. (Figure 23) This comes from differences in the thrust measurement, possibly originating in windspeed and direction. Both are not measured yet.
The torque measurement had less variation, resulting in a smaller prediction boundary. (Figure 24)
The higher pole count of the motor does not compensate the lower RPM of the motor, resulting in lower electrical field rotations than the smaller motors. This increases to the uncertainty of the RPM measurement and therefore, both coefficients.

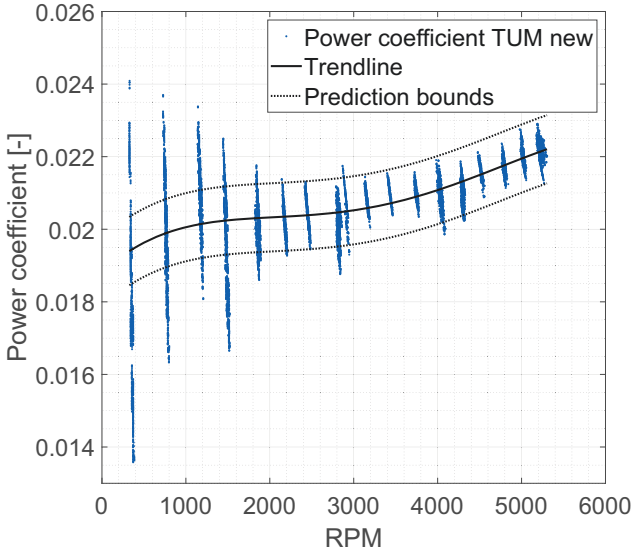

FIG 24. Power coefficient over RPM for the T-Prop 28" x 9.2" (blue) with its 95 % prediction bounds as dotted blue lines.

5. DISCUSSION

The graphs in Section 4 showed that there are still deviations in the measurement. Especially the RPM measurement is still not precise enough. Especially at low rpm, the RPM sensor needs to be tweaked even further.
While the data at UIUC was taken inside a closed wind tunnel, the presented data was measured in an open measurement container or even outside. While a lower instream velocity would usually suggest a higher thrust coefficient, this might change close to the stall of the propeller. Personal communication with University of Beira Interior showed, that real static thrust measurements are not possible with their wind tunnel setup. Comparable problems could be expected for the UIUC data as well.

Beside measurement errors there are some possibilities for the differences between the SUPER and Graupner propeller:

- Different plastic - carbon fiber composition
- Slightly different shape at the leading edge or trailing edge due to the manufacturing process
- Changes in the Graupner propeller due to storage conditions

Calibrating the load cell was performed by loading one axis at a time. In reality, thrust and torque are loaded simultaneously. With 6-axis load cells the crosstalk between their axis is usually defined in the datasheet. Unfortunately, this is unknown for the used 2 axis load cell.
Finally, some of the given datasheet values seem to be too optimistic. Especially the temperature drifts were higher than expected and the sensitive differential heating of the load cell could create problematic measurement scenarios even after the introduced hardware changes.

5.1. Ongoing tasks

Work on the test bench is still ongoing. This paper already showed a lot of progress, but the results are not yet sufficient. The RPM sensor is currently the most important task. A different filtering method with analog low-pass signal filtering and more advanced digital filters is currently planned.
A new microcontroller software for the RPM measurement will include the timing between the motor phase signal and when the data is sent to the measurement computer. This should eliminate the steps currently observed in the rotational speed.
A 2-axis calibration of the load cell is very time consuming. Before that, some basic tests will be performed to check if there is any crosstalk between the axis.
The components need to be rearranged to reduce the profile of the test bench, allowing for bigger propellers in the measurement container. Afterwards a more comprehensive comparison of different measurement locations can be performed.

High quality PCBs will replace the current prototypes for increased stability and reliability.
The final goal is to prepare the test bench for at least semi-automatic measurement in a wind tunnel. This includes tests on how to adapt the "random" input file and how to zero-offset the load cell in the wind tunnel. Early tests can maybe already show the effect of a closed wind tunnel for static testing instead of the used open environment.
Motor performance and efficiency can be calculated with the recorded data as well. This will be examined as well in future measurement campaigns.

5.2. Lessons learned

- The equipment should have reasonable range for the use cases. It might even be better to have two separate load cells for different measurement ranges. It helps to account for additional unexpected deviations and external interference in a non-perfect environment.
- Use digital sensors where possible. It avoids having analog signal interference and creates less problems with noise.
- Keep the sensor cables short. Better use an additional local acquisition devise next to the sensors instead of long cables. Most probably, time-correlating the data files afterwards is necessary anyway. One more data source does not add a lot of work.
- Shielded cables should be used from the beginning. Standard cables like ethernet CAT cables make this process easier by providing a standardized and simple connector. Creating the PCBs and additional components might cost a little more and it might be more work to create the PCBs, but it saves time through reducing the induced noise.
- Analog filtering of signals should be considered from the beginning to be able to comply with the Nyquist frequency.
- Test everything against external hardware. Even if it worked fine for years everywhere else. It might not be the case in the new project. The RPM sensors are a fine example. With the test bench they were initially unreliable despite unproblematic use in other applications for years.
- On the software part it was a good idea to keep it as simple as possible and divide it into reasonable parts. Measuring should be easy, with no crashes or lost communication. Ideally the amount of recorded data is as small as needed to speed up post processing time. The post processing script was actually modified a lot during the testing campaign and, therefore, a good thing to be completely independent of the measuring software.
- When using data from different sources, recorded to different files, the data fusion is one of the most critical steps. What timing accuracy is need, how to timestamp each dataset and what strategy is used to fuse all the data into one combined set afterwards needs to be defined beforehand to reduce later modifications.

6. CONCLUSION

In this investigation, the aim was to assess the accuracy of the existing test bench, identify the problematic parts and modify the measurement setup for more reliable data collection.
It was shown that the changes to the test bench increased its accuracy and reliability. Unfortunately, some deviations still persist. Future work will determine how much of the deviation is originating from errors during the measurement or coming from the different environment where the propeller was measured.
The generated propeller coefficients can be used to optimize UAVs. Especially the presented power coefficient allows for relatively precise calculations.
The measurement of big propellers is especially helpful for the hover propellers on heavy VTOL UAVs and will be continued in the future.

Contact address:

christian.rieger@tum.de

References

[1] Christian Rieger. *Experimentelle Untersuchung von Auswirkungen von Objekten im Zu- und Abstrom von Propellern für Multirotor UAV*. Semesterarbeit, Technische Universität München, München, 2017.

[2] Anne Lena Holzäpfel. *Calibration and Verification of a Static Thrust Test Bench Using Multiple Propellers*. Bachelor thesis, Technische Universität München, München, 2021.

[3] Robert W. Deters, G. Krishnan Ananda, Kumar Gavin, and Michael S. Selig. Reynolds number effects on the performance of small-scale propellers. In *32nd AIAA Applied Aerodynamics Conference, 16-20 June 2014, Atlanta, Georgia*, 2014. DOI: 10.2514/6.2014-2151.

[4] Or D. Dantsker, Marco Caccamo, Robert W. Deters, and Michael S. Selig. Performance testing of aero-naut cam folding propellers. In *AIAA Aviation 2020 Forum, 15-19 June 2020, Virtual Event*, 2020. DOI: 10.2514/6.2020-2762.

[5] John B. Brandt, Robert W. Deters, G. Krishnan Ananda, Or D. Dantsker, and Michael S. Selig. UIUC Propeller Data Bite, Vols 1-3, 2020. Available from: `https://m-selig.ae.illinois.edu/props/propDB.html` [Accessed 9th November 2020].

[6] M.A.R. Silvestre, J. Morgado, P. Alves, P. Santos, P. Gamboa, and J. C. Páscoa. Propeller performance measurements at low reynolds num-

bers. *International Journal of Mechanics*, 9:154–166, 2015.

[7] Monal Merchant and L. Scott Miller. Propeller performance measurement for low reynolds number UAV applications. In *44th AIAA Aerospace Sciences Meeting and Exhibit, 9-12 January 2006, Reno, Nevada*, 2006. DOI: 10.2514/6.2006-1127.

[8] Armin Ghoddoussi and L. Scott Miller. A preliminary database for low reynolds number propeller performance validations. In *51st AIAA/SAE/ASEE Joint Propulsion Conference, 27-29 July 2015, Orlando, Florida*, 2015. DOI: 10.2514/6.2015-4112.

[9] Matthew McCrink and James W. Gregory. Blade element momentum modeling of low-re small uas electric propulsion systems. In *33rd AIAA Applied Aerodynamics Conference, 22-26 June 2015, Dallas, Texas*, 2015. DOI: 10.2514/6.2015-3296.

[10] Sebastian Speck, Sebastian Herbst, Hyemin Kim, Franz-Georg Stein, and Mirko Hornung. Development, startup operations and tests of a propeller wind tunnel test rig. In *33rd AIAA Applied Aerodynamics Conference, 22-26 June 2015, Dallas, Texas*, 2015. DOI: 10.2514/6.2015-2578.

[11] Interface Inc. *Model 1216 Axial Torsion Load Cell*.

[12] SM Modellbau. Brushless drehzahlsensor, 2021.

[13] Pololu. Micro maestro 6-channel usb servo controller (assembled), 2021.

[14] K. Deergha Rao and M.N.S. Swamy. *Digital Signal Processing: Theory and Practice*. Springer, Singapore, 2018. ISBN: 978-981-10-8080-7. DOI: 10.1007/978-981-10-8081-4.

[15] Richard S. Figliola and Donald E. Beasley. *Theory and Design for Mechanical Measurements*. Wiley, New York, NY, 3. edition, 2000. ISBN: 0471350834.

[16] John R. Taylor. *Fehleranalyse: Eine Einführung in die Untersuchung von Unsicherheiten in physikalischen Messungen*. VCH, Weinheim, 1. edition, 1988. ISBN: 3-527-26878-2.

[17] STMicroelectronics. *MEMS pressure sensor: 260-1260 hPa absolute digital output barometer: Datasheet - production data*, 2014.

[18] Sensirion. *Datasheet SHT3x-DIS*, 2015.

[19] Texas Instruments. *TMP117 high-accuracy, low-power, digital temperature sensor with SMBus™- and I2C-compatible interface*, 2019.

[20] Interface Inc. *Model SGA Strain Gauge Transducer Amplifier: User Manual*, 2007.